Dalton Transactions

Insights into the solvent-assisted degradation of organophosphorus compounds by a Zr-based metal-organic framework

Journal:	*Dalton Transactions*
Manuscript ID	DT-COM-09-2019-003710.R1
Article Type:	Communication
Date Submitted by the Author:	02-Oct-2019
Complete List of Authors:	Harvey, Jacob; Sandia National Laboratories, Geochemistry Pearce, Charles; Sandia National Laboratory, Hall, Morgan; Edgewood Chemical Biological Center, Bruni, Eric; Combat Capabilities Development Command Chemical Biological Center DeCoste, Jared; jared.b.decoste2.ctr@mail.mil, Aberdeen Proving Ground Sava Gallis, Dorina; Sandia National Laboratories, Department of Nanoscale Sciences

COMMUNICATION

Insights into the solvent-assisted degradation of organophosphorus compounds by a Zr-based metal-organic framework

Received 00th January 20xx,
Accepted 00th January 20xx

DOI: 10.1039/x0xx00000x

Jacob A. Harvey,[a] Charles J. Pearce,[b] Morgan G. Hall,[c] Eric J. Bruni,[c] Jared B. DeCoste,[c] Dorina F. Sava Gallis[b*]

The degradation of a chemical warfare agent simulant using a catalytically active Zr-based metal-organic framework (MOF) as a function of different solvent systems was investigated. Complementary molecular modelling studies indicate that the differences in the degradation rates are related to the increasing size in the nucleophile, which hinders the rotation of the product molecule during degradation. Methanol was identified as an appropriate solvent for non-aqueous degradation applications and demonstrated to support the MOF-based destruction of both Sarin and Soman.

Efficient catalytic degradation of chemical warfare agents (CWAs), a class of highly toxic chemicals, is an ongoing challenge.[1] While significant progress on the hydrolysis degradation of these compounds has been made in recent years,[2] these techniques are mainly incompatible with applications where corrosion would occur (i.e.; sensitive electronics). Therefore, a pressing need remains to develop technologies that can degrade CWAs in non-aqueous environments.

Metal-organic frameworks (MOFs) have been shown to strongly adsorb and catalytically degrade CWAs.[3, 4] The large majority of these studies have focused on the degradation mechanism and rates in aqueous environments, yet few studies have looked at the methanolysis reaction for either CWAs or their simulants.[5, 6] Recently we showed that UiO-66, a prototypical Zr-based MOF,[7] degrades GB and its simulant dimethyl 4-nitriphenylphosphate (DMNP) in methanol.[6]

In an effort to explore the effect of solvent on the catalytic activity of MOF-based degradation of organophosphorus compounds, here we extend our original study to a wider range of non-/aqueous solvents using a related Zr MOF, based on the same catalytically active $Zr_6O_4(OH)_4$ metal clusters as in UiO-66. In this structure, the molecular building blocks are connected by a tetracarboxylic acid linker, namely 1,2,4,5-tetrakis(4-carboxyphenyl)benzene (TCPB). The resulting three-dimensional framework is characterized by potentially accessible voids along the [001] direction, 10 Å x 21 Å (Fig. 1a), and along the [100] direction, 9.5 Å x 4.5 Å (Fig. 1b). The ZrTCPB MOF used here was obtained via a unique synthetic route (see ESI† for full experimental details),[8] yielding a nanosized crystalline material, as confirmed by TEM studies, Fig. 1c.

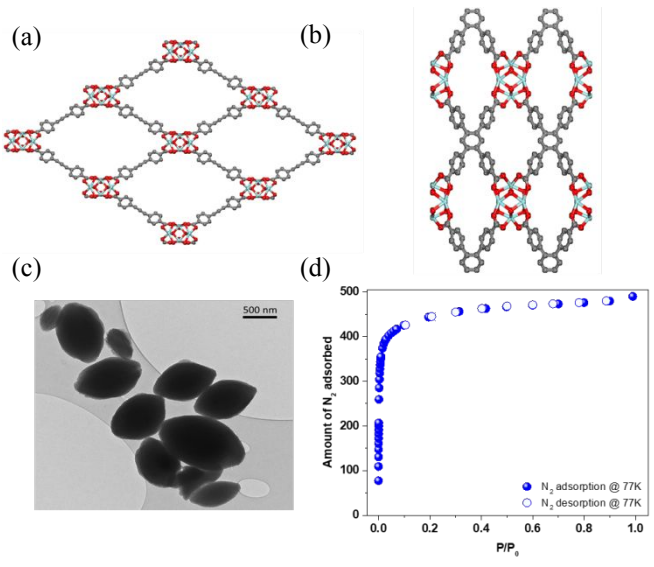

Fig. 1 (a,b) Ball-and-stick representation of the channels in ZrTCPB along two different directions. Atoms color scheme: Zr= blue; C= grey; O= red; H= white; (c) representative TEM; (d) N_2 sorption isotherm measured at 77K.

Permanent porosity was assessed on the as made sample via guest exchange in methanol over 3 days, and then activation

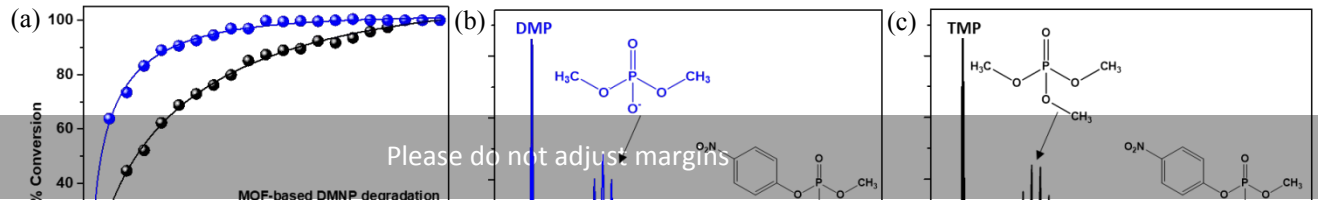

[a] Geochemistry Department, Sandia National Laboratories, Albuquerque, NM 87185, USA.
[b] Nanoscale Sciences Department, Sandia National Laboratories, Albuquerque, NM 87185, USA. E-mail: dfsava@sandia.gov
[c] Combat Capabilities Development Command Chemical Biological Center, U.S. Army Research, Development and Engineering Command, 8198 Blackhawk Road, Aberdeen Proving Ground, MD 21010 USA.

†Electronic Supplementary Information (ESI) available: Full experimental and computational details, PXRD of pristine and HCl washed MOF samples, N2 adsorption pre- and post-HCl wash, DMNP reaction rate for various MOF:DMNP ratios, solvent only degradation of DMNP, and structural figures of H_2O degraded GB in ZrTCPB. See DOI: 10.1039/x0xx00000x

under vacuum on a Micromeritics ASAP 2020 surface area and porosity analyzer (30°C for 6 hrs followed by thermal treatment to 150°C for 12 hrs, ESI†). The resulting specific BET surface area was calculated to be 1330 m^2/g (Fig. S1, ESI†). To ensure complete removal of the modulator agent (fluorobenzoic acid), a subsequent procedure was employed consisting of immersion in a dimethylformamide (DMF)/HCl solution at 115°C for 12 hrs (ESI†).[9] Powder X-ray diffraction studies confirmed this procedure had no effect on the crystallinity of the structure (Fig. S2). As anticipated, upon sample re-activation, the specific BET surface area increased to 1740 m^2/g (Fig. 1d and Fig. S2, ESI†).

Further, we investigated the ZrTCPB-based degradation of DMNP in water, methanol (MeOH), isopropyl alcohol (IPA), and hydrofluoroether (HFE); as well as sarin (GB) and soman (GD) in MeOH. To assess the degradation of CWA simulant and agents, *in situ* ^{31}P NMR spectroscopy was employed; experiments were conducted at 50°C. In order to access the optimal reaction conditions, we explored, in depth, the MOF:DMNP ratio (Table S1, Fig. S3, ESI†). The best performance was obtained with a ratio of 28.4% and therefore used throughout the remainder of this study.

The time evolution of DMNP degradation in water, MeOH, IPA, and HFE is shown in Fig. 2. The fastest degradation is observed in water, closely followed by MeOH. Interestingly, little to no reaction is noted with IPA (~ 5 % conversion) and HFE (no conversion). To be noted, DMNP does not degrade at all in MeOH alone and degrades very slowly in neat H_2O (Fig. S4, ESI†), confirming the critical catalytic activity native to the ZrTCPB MOF.

To confirm the identity of the products resulting from the hydrolysis and methanolysis reactions, respectively, ^1H-coupled ^{31}P NMR was employed, Fig. 2b, c. The peak corresponding to the DMNP hydrolysis decomposition product is split into a 7-peak multiplet (inset of Fig. 2c), identified as dimethyl phosphate anion (DMP), highlighted by 6 ^1H-^{31}P interactions. The methanolysis product showed a multiplet split 10 ways (inset of Fig. 2b), corresponding to 9 identical ^1H-^{31}P interactions, and identified as trimethyl phosphate (TMP).

Given that DMNP fully degrades in MeOH and represents an appropriate CWA simulant, [6,10-12] we further explored the utility of the ZrTCPB system for the destruction of GB and GD. *Caution! Experiments using GB and GD should be run by trained personnel using appropriate safety procedures only.* The ZrTCPB-based degradation of GB, GD, and DMNP in MeOH is shown in Fig. 3. Interestingly, the degradation rates of GB and GD in MeOH are very similar (~40% conversion after 800 min). This finding contrasts recent results which indicate that the hydrolysis of GB occurs five times faster than that of GD on four related Zr-based MOFs.[10] It should be noted that these reactions were all conducted in aqueous buffered solutions, which were shown to be heavily pH dependent. Additionally, it is important to note that the DMNP reaction kinetics are significantly faster than that of both GB and GD under the same testing conditions, reaching 100% conversion after 800 min.[6] Notably, these results differ from findings from our previous study, [6] where UiO-66-based methanolysis of DMNP was slower than that of GB (studies conducted at 25°C). This suggests that both temperature and MOF:agent ratio significantly influence the reaction kinetics.

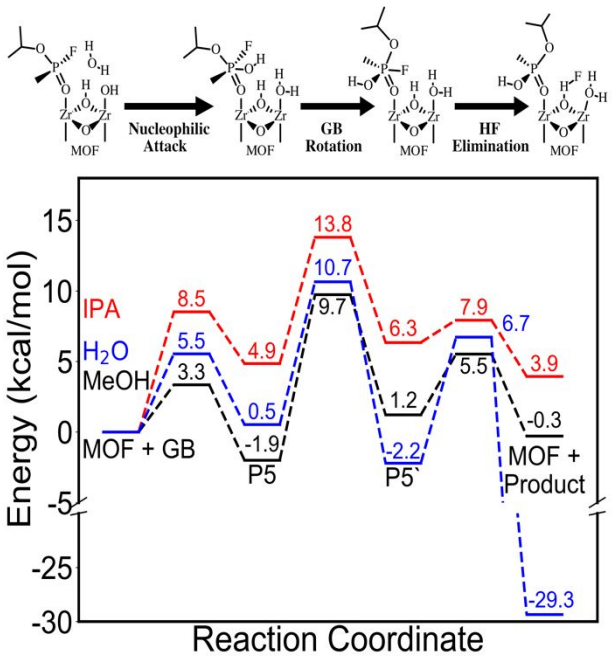

Fig. 4 Reaction pathway energies for the degradation of GB on ZrTCPB in H2O (blue), Fig. 3 ZrTCPB sMeOH (black), and IPA (red). The energies shown for each transition state and GB (red) in Meintermediate are in kcal·mol^{-1} units. A 2D representation of the degradation pathway is depicted in the top image.

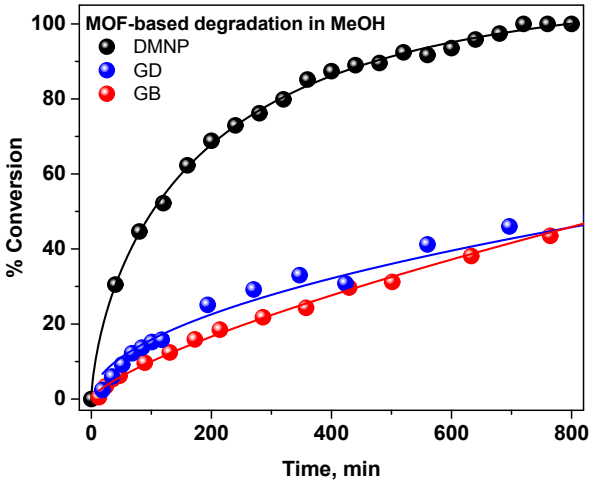

In an effort to gather additional insights on the molecular level origins of the reaction mechanism of GB and GD in each solvent we implemented density functional theory (DFT) calculations to determine the full degradation pathway. Specifically, we used the climbing image nudge elastic band method[13, 14] to calculate the electronic energies along the reaction pathway for GB and GD degradation on ZrTCPB with a single water, MeOH, and IPA solvent molecule. All calculations were performed on the three-dimensional periodic structure using the Vienna Ab-Initio Simulation Package plane wave electronic structure code (See ESI for full computational

details).[15-18] The computational approach outlined here and in the ESI was recently validated against experimental in-situ infrared spectroscopy of GB bound in UiO-66;[19] backing up previous claims made regarding more accurate binding energies using periodic approaches.[20] The reaction pathway considered was that identified by Troya for GB degradation in UiO-66.[21] Results for the degradation pathway of GB in the three solvents are shown in Fig. 4. The energetics of GD degradation are very similar to GB for all solvents (Fig. S5, ESI†) with slight variances in observed barriers, in agreement with experimental reactivities. Structures for all reactants, products, intermediates and transition states are given in Fig S6-S11 (ESI†).

The degradation mechanism goes through a three-step process. Degradation is initiated with the solvent molecule hydrogen bound to the μ_3-OH and the GB/GD molecule bound to the undercoordinated Zr metal (MOF + GB/GD). The first step involves a solvent molecule nucleophilic attack at the phosphorus atom by to form a five-coordinated phosphorus complex (P5). A Berry pseudorotation is then required to move the F atom from the equatorial to axial position (P5`). Finally, the F atom is eliminated to form HF and the GB/GD degradation product (MOF + product).

In all calculations the Berry pseudorotation step is the rate limiting step, producing barriers typically ~10 kcal · mol^{-1}, whereas we observe barriers of ~3-8 kcal · mol^{-1} for the nucleophilic attack step. The barrier for F elimination is typically the smallest at ~1-2 kcal · mol^{-1}. This pseudorotation step involves a large rotation of the GB/GD molecule at the active site, which is stabilized via a hydrogen bond between the F atom and the μ_3-OH. Given the sterics near the active site due to the organic linkers it is unsurprising that this barrier be quite large.

To the best of our knowledge, only one other study has considered this step in the degradation pathway of GB on Zr-based MOFs, in which only small metal clusters were considered where the linkers were truncated to formate groups. Given the lack of sterics in the cluster approach, the barrier for pseudorotation (1.67 kcal · mol^{-1}) was found to be much smaller than the nucleophilic attack barrier (16.5 kcal · mol^{-1}).[21] Other subsequent studies have solely considered the nucleophilic attack step in their calculation, despite the fact that most models now utilize 3D models in their calculations.[22-25] Recent works, utilizing a periodic approach, have calculated the full degradation of GB on Ti-based MOFs, however those calculations were performed without solvent where the rotation step is not observed.[26] The results depicted here clearly indicate that this step should be considered in modelling efforts for the solvent-assisted degradation of these molecules in MOFs.

In transitioning from water to MeOH, the resulting size of the degradation product is increased via the addition of methyl groups. The larger size increases the pseudorotation barrier in GB degradation from 10.2 kcal · mol^{-1} in H_2O to 11.6 kcal · mol^{-1} in MeOH, confirming the experimentally observed increased reaction kinetics in water. We note that the pseudorotation barrier in IPA is actually smaller than H_2O or MeOH, however, the degradation pathway in IPA contains multiple large barriers and thermodynamic penalties. The necessity to overcome two large reaction barriers in order to degrade the target molecule likely causes the lack of reactivity experimentally observed in this solvent. The first barrier likely combines multiple effects including pKa, as a proton is transferred to the ZrOH group, and nucleophilic strength. On-going calculations are focused on isolating the effect of each of these features.

One might expect the reaction rate of DMNP to be slower than GB given the larger size, however in this study we observe the opposite experimentally (Fig. 3). In our calculations the size of the solvent has a greater effect on the MOF structure than the size of the degrading molecule. More specifically, a twist in organic linkers at the active site is observed and the magnitude of the twist increases as solvent size increases. Whereas the magnitude of the twist is nearly equivalent for GB and GD in similar solvents, despite the larger size of the GD molecule (Fig. S12 and Table S3 for relevant structures indicating linker twisting and dihedral angle changes for GB and GD in all solvents, ESI†).

Interestingly there is a large thermodynamic advantage in the water-based degradation of GB, which likely aids in driving future reactions. Our modelling efforts confirm the experimentally observed deprotonated product in water, isopropyl methylphosphonic acid. Three stable products were identified: (i) first, in which the leaving F atom shares the proton on the μ_3-OH, Zr-chelated water, and product; (ii) second, in which the F atom shares the proton on the μ_3-OH and product, and (iii) third, in which the F atom shares the proton on the μ_3-OH and Zr-chelated water. The relative energies for these products are 0.0, 4.9, and 28.4 kcal · mol^{-1} (Fig. S13 for structures, ESI†). Only the third structure mentioned remains protonated but is much higher in energy. The structure in which the F atom is shared between the μ_3-OH and product (Fig. S11 b, ESI†) is used in the reaction profile diagram as it is most comparable structurally to the products observed for MeOH and IPA degradation.

In summary, here we investigated the solvent effects (water, MeOH, IPA and HFE) on the MOF-based degradation of DMNP, a relevant simulant for GB and GB chemical warfare agents. It was found that the Zr-based MOF chosen here (ZrTCPB) successfully degrades DMNP in both water and MeOH. The hydrolysis reaction proceeds faster than that in MeOH. Further, this material promotes the degradation of both GB and GD in MeOH. Notably, no degradation was observed in either IPA or HFE with DMNP.

Complementary molecular modelling studies were employed to calculate the electronic energies along the reaction pathway for the degradation of GB and GD in water, MeOH and IPA. Results indicate that the rotation of the molecule is hindered near the active site and that bulkier nucleophiles are responsible for decreased degradation rates. Our results indicate that this rarely considered pseudorotation step in the degradation pathway is imperative to include when evaluating trends across different metals, ligands, or solvents.

The authors would like to acknowledge Dr. Mark Kinnan for helpful discussions and Dr. Todd Alam for technical guidance with NMR experiments. This work is supported by the Laboratory Directed Research and Development Program at

Sandia National Laboratories. Sandia National Laboratories is a multimission laboratory managed and operated by National Technology and Engineering Solutions of Sandia, LLC., a wholly owned subsidiary of Honeywell International, Inc., for the U.S. Department of Energy's National Nuclear Security Administration under contract DE-NA-0003525. The views expressed in this article do not necessarily represent the views of the U.S . Department of Energy or the United States Government.

Conflicts of interest

There are no conflicts to declare.

Notes and references

1. M. Enserink, *Science*, 2013, **341**, 1050-1051.
2. Y. J. Jang, K. Kim, O. G. Tsay, D. A. Atwood and D. G. Churchill, *Chem. Rev.*, 2015, **115**, PR1-PR76.
3. J. B. DeCoste and G. W. Peterson, *Chem. Rev.*, 2014, **114**, 5695-5727.
4. N. S. Bobbitt, M. L. Mendonca, A. J. Howarth, T. Islamoglu, J. T. Hupp, O. K. Farha and R. Q. Snurr, *Chem. Soc. Rev.*, 2017, **46**, 3357-3385.
5. M. J. Katz, J. E. Mondloch, R. K. Totten, J. K. Park, S. T. Nguyen, O. K. Farha and J. T. Hupp, *Angew. Chem. Int. Ed.*, 2014, **53**, 497-501.
6. D. F. Sava Gallis, J. A. Harvey, C. J. Pearce, M. G. Hall, J. B. DeCoste, M. K. Kinnan and J. A. Greathouse, *J. Mater. Chem. A*, 2018, **6**, 3038-3045.
7. J. H. Cavka, S. Jakobsen, U. Olsbye, N. Guillou, C. Lamberti, S. Bordiga and K. P. Lillerud, *JACS*, 2008, **130**, 13850-13851.
8. M. Lammert, H. Reinsch, C. A. Murray, M. T. Wharmby, H. Terraschke and N. Stock, *Dalton Trans.*, 2016, **45**, 18822-18826.
9. Y. Liu, S.-Y. Moon, J. T. Hupp and O. K. Farha, *ACS Nano*, 2015, **9**, 12358-12364.
10. A. M. Ploskonka and J. B. DeCoste, *J. Hazard. Mater.*, 2019, **375**, 191-197.
11. I. Matito-Martos, P. Z. Moghadam, A. Li, V. Colombo, J. A. R. Navarro, S. Calero and D. Fairen-Jimenez, *Chem. Mater.*, 2018, **30**, 4571-4579.
12. M. Agrawal, D. F. Sava Gallis, J. A. Greathouse and D. S. Sholl, *J. Phys. Chem. C*, 2018, **122**, 26061-26069.
13. G. Henkelman and H. Jónsson, *J. Chem. Phys.*, 2000, **113**, 9978-9985.
14. G. Henkelman, B. P. Uberuaga and H. Jónsson, *J. Chem. Phys.*, 2000, **113**, 9901-9904.
15. G. Kresse and J. Hafner, *Phys. Rev. B*, 1993, **47**, 558-561.
16. G. Kresse and J. Hafner, *Phys. Rev. B*, 1994, **49**, 14251-14269.
17. G. Kresse and J. Furthmuller, *Comp. Mater. Sci.*, 1996, **6**, 15-50.
18. G. Kresse and J. Furthmuller, *Phys. Rev. B*, 1996, **54**, 11169-11186.
19. J. A. Harvey, M. L. McEntee, S. J. Garibay, E. M. Durke, J. B. DeCoste, J. A. Greathouse and D. F. Sava Gallis, *J. Phys. Chem. Lett.*, 2019, DOI: (accepted).
20. J. A. Harvey, J. A. Greathouse and D. F. S. Gallis, *J. Phys. Chem. C*, 2018, **122**, 26889-26896.
21. D. Troya, *J. Phys. Chem. C*, 2016, **120**, 29312-29323.
22. M. R. Momeni and C. J. Cramer, *ACS Appl. Mater. Interfaces*, 2018, **10**, 18435-18439.
23. M. R. Momeni and C. J. Cramer, *Chem. Mater.*, 2018, **30**, 4432-4439.
24. M. Kalaj, M. R. Momeni, K. C. Bentz, K. S. Barcus, J. M. Palomba, F. Paesani and S. M. Cohen, *Chem. Commun.*, 2019, **55**, 3481-3484.
25. M. R. Momeni and C. J. Cramer, *J. Phys. Chem. C*, 2019, **123**, 15157-15165.
26. C. Vieira Soares, G. Maurin and A. A. Leitão, *J. Phys. Chem. C*, 2019, **123**, 19077-19086.

TOC

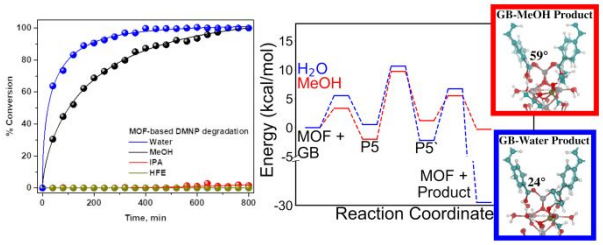

Insights into the MOF-based degradation of organophosphorus compounds in non-/aqueous solvents highlights the effect of solvent size on reaction rates.